Intermolecular Association of Tetrahydrofuran-2-carboxylic Acid in Solution: A Vibrational Circular Dichroism Study

Tom Kuppens,[†] Wouter Herrebout,[‡] Benjamin van der Veken,[†] and Patrick Bultinck*[,†]

Department of Inorganic and Physical Chemistry, Ghent University, Krijgslaan 281-S3, B-9000 Ghent, Belgium, and Department of Chemistry, University of Antwerp, Groenenborgerlaan 171, B-2020 Antwerp, Belgium

Received: February 11, 2006; In Final Form: June 27, 2006

Carboxylic acids are known for their strong intermolecular associations. With chiral carboxylic acids, this behavior can be studied using vibrational circular dichroism (VCD). Tetrahydrofuran-2-carboxylic acid **1**, a chiral building block for β-lactam antibiotics, is studied by emphasizing the effect of the dimerization. Experimental results indicate that for solutions of **1** in $CDCl_3$ and CS_2, a complex equilibrium exists between the monomers and dimers. B3LYP/aug-cc-pVTZ calculations are performed on both monomer and dimer structures. To simulate IR and VCD spectra, populations for monomer and dimers were approximated using a semiquantitative model. A good agreement between experimental and simulated spectra is obtained by taking into account both the monomeric and the dimeric structures, weighted using the experimentally determined populations.

Introduction

In this study tetrahydrofuran-2-carboxylic acid (**1**) is studied using vibrational spectroscopy including both unpolarized infrared (IR) and vibrational circular dichroism (VCD) spectroscopy. (*R*)-Tetrahydrofuran-2-carboxylic acid is a chiral building block for faropenem (7-(1-hydroxyethyl)-6-oxo-3-oxolan-2-yl-2-thia-5-azabicyclo[3.2.0]hept-3-ene-4-carboxylic acid),[1,2] a clinically effective nonnatural β-lactam antibiotic.[3]

In combination with density functional theory (DFT) calculations,[4] VCD spectroscopy allows the elucidation of the absolute configuration and the conformational behavior of chiral compounds.[5−7] By doing DFT calculations on a compound with known stereochemistry, one can simulate IR and VCD spectra and consequently compare them with experimental spectra. The IR spectra of enantiomers are identical but the VCD spectra, which are in essence differential IR spectra recorded with left and right circularly polarized infrared light, have intensities with opposite sign. As each vibrational transition band has a corresponding VCD band, each one of these bands can be compared with the simulated spectrum, allowing a very reliable assignment of the stereochemistry of the measured enantiomerically pure sample. At the same time, information about the primary conformations is obtained, as VCD is very sensitive to conformational change. The VCD method was proven very successful in the past[8−14] and further development in spectroscopic techniques and computational algorithms will further increase the reliability of this method.[15,16]

1 is a carboxylic acid, and these types of compounds are known to form intermolecular aggregates.[17,18] In the solid and liquid phase, associations mainly involve cyclic dimers. These are also formed in the gas phase and in solutions. In protic solvents, hydrogen bonding with solvent molecules appears concurrent to dimer formation.[19] As self-association considerably influences the conformational and vibrational properties of the molecules,[20−22] a suitable model has to be used when computing IR and VCD spectra. In the past, only a few studies were carried out on dimers, in which the focus was on relatively rigid structures.[23,24] A more recent and extensive paper[25] from He et al. describes a VCD study on α-(aryloxy)propanoic acid cyclic dimers; however, the equilibrium between monomer and dimer was not further investigated. Also, recently, Urbanová et al.[26] published a VCD study concerning a tetrameric dimethylbiphenyldicarboxylic acid structure. In both studies the calculations are performed with the B3LYP hybrid functional using the 6-31G* basis set.

In this study the computational level is extended, by means of the use of different functionals and larger basis sets. The focus of the present paper is first to establish whether the dimerization has an important effect on the experimental spectra. Second, it is investigated if this effect can be simulated using DFT calculations. Further, a semiquantitative model is defined to obtain estimates of monomer and dimer populations. Combining the semiquantitative populations and DFT results, the experimental IR and VCD will be assessed.

Experimental Methods

(*R*)-(+)-**1** ($\alpha_D^{20} = +30.0$ ($c = 0.34$, $CHCl_3$))[1] and (*S*)-(−)-**1** ($\alpha_D^{20} = -12.6$ ($c = 7.70$, H_2O)[27] were obtained from Acros with a 97.5% ee and were used without further purification. IR spectra are measured with a Bruker Vector 22 FTIR spectrometer. The VCD is measured with an IFS 66v FTIR spectrometer coupled to a PMA37 module, set up as described in Urbanová et al.[28] Long wave pass filters are used to select an operational frequency window to improve the signal-to-noise (S/N) ratio. Because it can induce large artifacts in the CO stretching region for compound **1**, the default 1830 cm^{-1} filter is unusable. Therefore, a 1960 cm^{-1} filter is used instead,[29] which allows measurement in the CO stretch region. As this filter has a rather high long-wave cutoff at 1250 cm^{-1}, the 1830 cm^{-1} filter is used for the measurements for (*R*)-(+)-**1** and (*S*)-(−)-**1** below

* Corresponding author. E-mail: Patrick.Bultinck@UGent.be.
[†] Ghent University.
[‡] University of Antwerp.

10.1021/jp0608980 CCC: $33.50
Published on Web 08/05/2006

TABLE 1: B3LYP/aug-cc-pVTZ Label, Pseudorotational Coordinates (q in Å and φ in deg), Key Dihedral Angles (τ_1 and τ_2 in deg), Relative Free Energies (ΔG^0 in kcal/mol) and Boltzmann Populations (% P, 298.15 K) for the Unique Monomer Minima of 1

label	q	φ	τ_1 $O^8C^6C^2O^1$	τ_2 $O^7C^6O^8H^9$	ΔG^0	% P
A	0.36	263	−3	182	0.00	40.59
B	0.36	76	4	180	0.16	31.14
C	0.34	106	154	−1	0.92	8.63
D	0.36	228	156	−1	1.06	6.73
F	0.36	240	−35	−1	1.08	6.61
E	0.34	100	−25	−1	1.10	6.30
G	0.34	105	153	177	6.02	0.00
H	0.36	227	154	176	6.11	0.00

1200 cm^{-1}, using CS_2 as solvent and KBr cell windows. Above 1200 cm^{-1}, the 1960 cm^{-1} filter is used, in combination with $CDCl_3$ as solvent and CaF_2 cell windows. The collection time for the VCD spectra is 90 min (3 × 30 min) each. The demountable cells are equipped with a 105 μm Teflon spacer. (*R*)-(+)-**1** and (*S*)-(−)-**1** are dissolved in $CDCl_3$ at a concentration of 0.42, 0.25 and 0.21 M. **1** has a low solubility in CS_2 and a solution is prepared at an approximate concentration of 0.11 M. Because both enantiomers are available, half-difference spectra[30] are computed as $(\Delta\epsilon_- - \Delta\epsilon_+)/2$, which provides spectra with an improved S/N ratio.

An infrared concentration study with (*R*)-(+)-**1** in $CHCl_3$ was performed using a KBr cell with a 200μm Teflon spacer.

Computational Methods

Geometry optimizations and calculations of the dipole strengths (D) and rotational strengths (R) are performed using Gaussian03.[31] In this study the B3LYP[32,33] hybrid functional is used, which has proven its reliability in the calculation of VCD intensities,[11,12,34] and the description of strong hydrogen bonded complexes.[35] The potential energy surface for the monomer and dimer are scanned using different methods, which are described in the section Conformational Search. The located monomer and dimer minima are optimized with the aug-cc-pVTZ basis set. This basis set was previously found capable of describing hydrogen bonded systems.[36] Six additional functionals (B1LYP, B3P86, B3PW91, B98, MPW1PW91, PBE1PBE)[37] are also

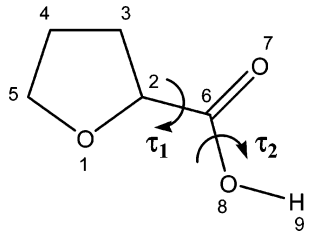

Figure 1. Depiction of **1** and definition of dihedral angles τ_1 and τ_2.

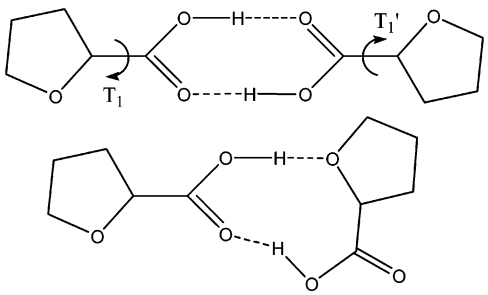

Figure 2. Two different possibilities to form cyclic dimers of **1**. Definition of dihedral angles T_1 and T_1'.

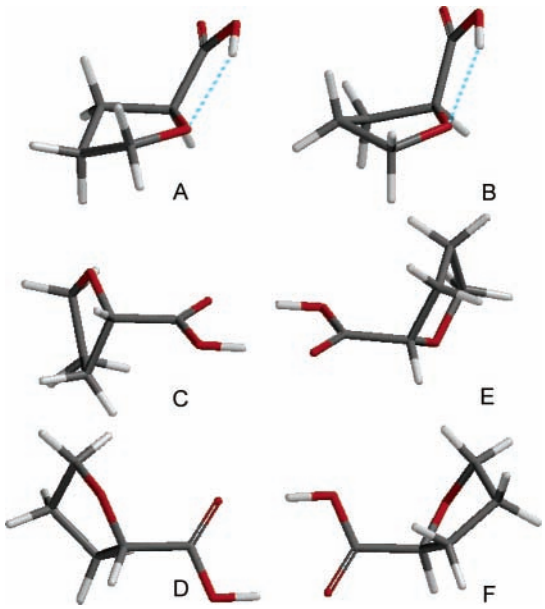

Figure 3. Model representations of the monomer conformations A−F and at the same time exemplary models of cyclic dimers EC and FD.

employed in combination with the 6-31++G** basis set for which the results can be found in Supporting Information.

Hessian matrixes, atomic polar tensors (APT) and atomic axial tensors (AAT) are calculated using gauge-including/invariant atomic orbitals (GIAOs),[38,39] at the same level as the optimization, allowing the calculation of dipole and rotational strengths. The free energy is calculated under the usual assumptions using standard thermochemical expressions.[40] A scaling factor of 0.980 is used to correct for the harmonic approximation.[41]

The calculations were performed on the Ghent Quantum Cluster (GQC) at Ghent University and CalcUA located at the University of Antwerp.

Conformational Search

The potential energy surfaces of the monomer and dimer of **1** with the *S* configuration were thoroughly analyzed to find the lower energy minima. For the monomer, a conformational analysis was done using MM3[42] and MM4[43] stochastic search methods, for which the implementation is described in more detail in earlier work,[11] and a Monte Carlo search using the MMFF[44] force field. All unique minima were subsequently optimized on the B3LYP/6-31G* level. A systematic B3LYP/6-31G* DFT search was also performed, which did not yield any new minima. The unique B3LYP/6-31G* minima were further optimized using the aug-cc-pVTZ basis set. For the located minima, the conformational description is given in Table 1. To describe the tetrahydrofuran (THF) ring conformations, Cremer−Pople pseudorotational coordinates[45] are used as defined in

$$z_i = \sqrt{\frac{2}{5}} \cdot q \cos\left(\frac{4\pi(i-1)}{5} + \varphi\right) \quad \text{with} \quad \sum_{i=1}^{5} z_i^2 = q^2 \quad \text{and} \quad \varphi \in [0, 360] \quad (1)$$

The puckering amplitude q describes the degree of ring puckering, and the pseudorotational phase angle φ describes the mode of ring puckering.[46] The position of the carboxyl substituent relative to the THF ring is given by τ_1. The configuration of the carboxyl group is specified by τ_2 (see Figure

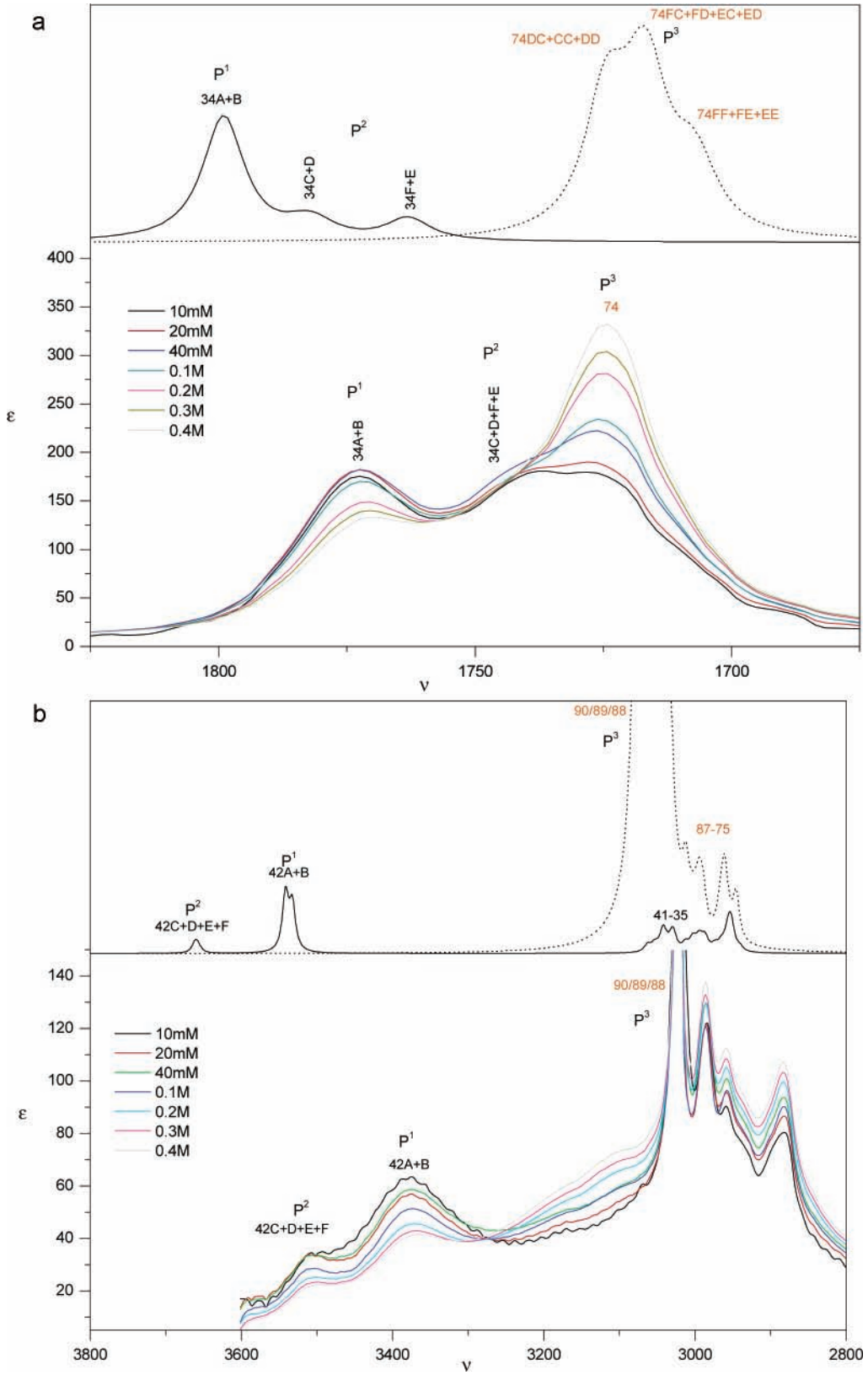

Figure 4. IR spectra of (*R*)-(+)-**1** in $CHCl_3$ for different concentrations varying between 0.4 M and 10 mM in the CO stretch (a) and OH stretch (b) region concurrent with the B3LYP/aug-cc-pVTZ simulated spectra for monomer (solid line) and dimer (dotted line) and assignments. Intensities in molar absorptivity units, frequencies in cm^{-1}.

1). τ_2 is found to be ~0° and ~180°; that is, the hydroxyl group can be orientated respectively cis or trans relative to the carbonyl group.

For the dimer of **1**, an MM3 and MM4 stochastic search was performed. This search yielded two relatively stable classes of geometries, which are given schematically in Figure 2. The most stable dimer is the classical one in which the two carboxylic acid groups form a strong hydrogen bonded association (Figure 2a). Cyclic associations are also observed in which the THF oxygen of one monomer is involved in forming cyclic dimers

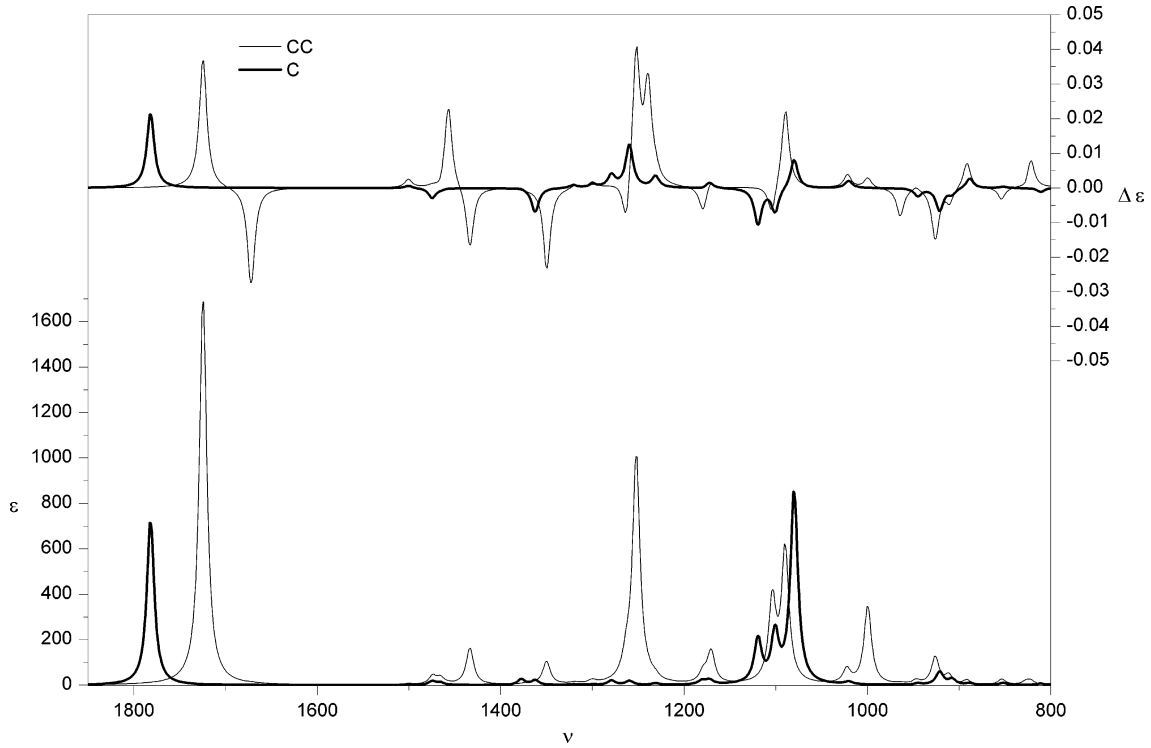

Figure 5. Single conformational spectra for monomer conformation C (thick solid line) and dimer conformation CC (solid line). Intensities and differential intensities in molar absorptivity units, frequencies in cm^{-1}.

TABLE 2: B3LYP/aug-cc-pVTZ Label, Symmetry, Pseudorotational Coordinates (q in Å and φ in deg), Key Dihedral Angles (T in deg), Relative Enthalpies (ΔH^0 in kcal/mol), Relative Free Energies (ΔG^0 in kcal/mol) and Boltzmann Populations (% P, 298.15 K) for the Unique Dimer Minima of 1

label		q_1	φ_1	T_1 $O^8C^6C^2O^1$	q_2	φ_2	$T_{1'}$ $O^{8'}C^{6'}C^{2'}O^{1'}$	ΔH^0	ΔG^0	% P
DC	C_1	0.36	232	156	0.34	102	156	0.06	0.00	24.2
FC	C_1	0.36	237	−35	0.34	108	155	0.12	0.19	17.5
EC	C_1	0.33	100	−29	0.34	105	156	0.27	0.52	10.1
CC	C_2	0.34	103	155	0.34	103	155	0.09	0.57	9.3
FD	C_1	0.36	237	−34	0.36	232	155	0.04	0.58	9.1
FF	C_2	0.36	238	−37	0.36	238	−37	0.37	0.59	8.9
ED	C_1	0.34	96	−31	0.36	232	154	0.23	0.63	8.4
FE	C_1	0.36	240	−36	0.34	105	−26	0.58	0.91	5.2
DD	C_2	0.36	234	154	0.36	234	154	0.00	0.94	5.0
EE	C_2	0.34	101	−27	0.34	102	−27	0.75	1.40	2.3

(Figure 2b). Noncyclic dimers with only one OH···O hydrogen bond were located as well but were discarded due to their high energy.[47] Further optimization at the 6-31++G** level showed that the dimers, in which the THF oxygen is involved, have a relative free energy of at least 5.5 kcal/mol compared to the other more stable carboxylic acid bonded cyclic dimers.

Consequently, it can be concluded that, when the dimers are considered, the classic cyclic dimers are most contributing. As the stochastic search did not yield many cyclic dimer geometries, a B3LYP/6-31++G** systematic search was performed in which T_1 and T_1' (the position of the carboxyl substituent relative to THF for the dimers as defined in Figure 2) were varied in a 30° grid for different values of q and φ for both THF rings. Using this approach, a total of 10 unique minima were located. These geometries were further optimized at the aug-cc-pVTZ level, for which the conformational description is given in Table 2.

It can be seen that each of these dimers are in fact combinations of monomer geometries, more precisely, the 4 monomers of **1** that have a cis carboxylic acid group configuration (C, D, E and F) and that are conformationally capable of forming cyclic dimers. However, clearly not all monomer geometries for **1** are able to form dimer structures as can be seen in Figure 3, as these are intramolecular hydrogen bonded structures in which the trans carboxylic OH interacts with the THF oxygen. There are also two trans carboxylic monomer structures located in which no intramolecular hydrogen bonding is present (conformation G and H in Table 1). Because of their high energies these minima are not significant.

If the relative enthalpy is compared to the relative free energy of the dimer structures, a different order can be observed. This is due to the various entropy contributions of each dimer minimum, e.g., dimers structures with C_2 symmetry have a lower rotational entropy contribution compared to C_1 structures.

Results and Discussion

In Figure 4a, the CO stretch region of the IR spectrum is presented for (*R*)-(+)-**1** solutions in $CHCl_3$, with typical concentrations varying between 0.01 and 0.40 M. Two intense bands can be observed in this region, with a rather large frequency separation, which, in the case of carboxylic acids, is often an indication for coexistence of dimer and monomer in solution.[48] This is confirmed in the OH stretch region, given in Figure 4b, in which two monomer bands can be observed near 3390 and 3500 cm^{-1} and a broad dimer band near 3000 cm^{-1}. In both the CO and OH stretch region the bands can be identified on the basis of DFT results. In Figure 4 the monomer and dimer calculated spectra are concurrently given (Tables S4 and S5 in Supporting Information describe the fundamentals for monomer and dimer conformations). From these data it can be seen that band P^1 can be assigned to the monomer with conformations A and B and P^2 to the cis-configured monomer (C, D, E and F). For conformations A and B, the carbonyl stretch frequency is somewhat higher and the hydroxyl stretch frequency is somewhat lower compared to the non-hydrogen bonded monomers

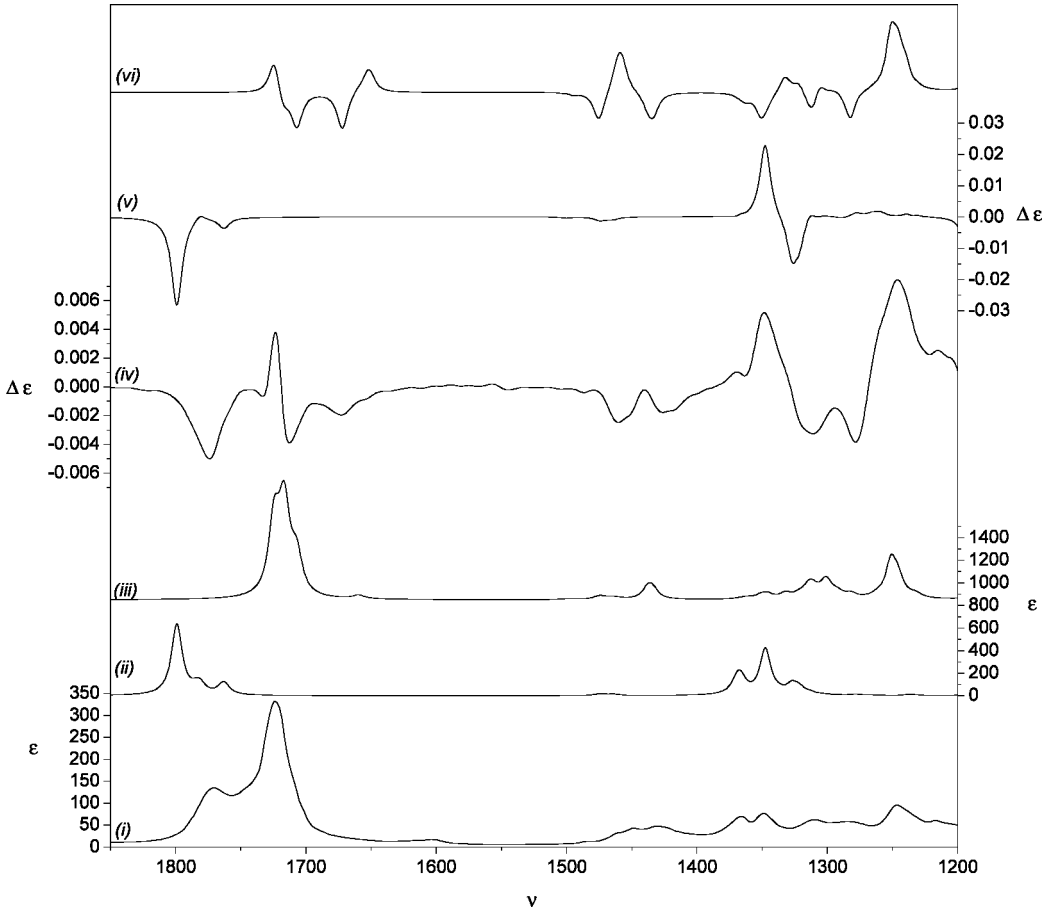

Figure 6. Experimental IR (i) and half-difference VCD (iv) spectrum for 0.42 M (*S*)-(−)-**1** in $CDCl_3$. Simulated IR/VCD B3LYP/aug-cc-pVTZ monomer (ii)/(v) and dimer (iii)/(vi) spectra are given. Intensities and differential intensities in molar absorptivity units, frequencies in cm^{-1}.

C, D, E and F. Also, the intensity of the hydrogen bonded monomer bands is higher compared to the cis configured monomers. These findings agree with the B3LYP intensities and populations. Further, band P^3 can be ascribed to the dimer conformations in the same manner. The typical concentration dependence of the three bands also confirms the assignment of monomer and dimer bands.

Solutions in CS_2 are also studied to extend the VCD frequency range. For (*R*)-(+)-**1** in CS_2, three carbonyl stretch bands can be observed (Figure S1 in Supporting Information), similar to the $CHCl_3$ spectra: P^1 centered at 1784 cm^{-1}, P^2 centered at 1756 cm^{-1} and P^3 at 1722 cm^{-1}. It is interesting to observe that these values, compared to the CO stretch frequencies in $CHCl_3$, are shifted to lower wavenumbers by ~11 cm^{-1}. Furthermore, the intensity ratios P^3/P^1 and P^3/P^2 are higher compared to the corresponding ratios in the $CHCl_3$ spectra. As the solubility of **1** in CS_2 is low, it was difficult to get solutions with accurate concentrations.

As it is clear now that both monomers and dimers are present in solution, these have to be taken into account when the spectra for **1** are simulated. IR and VCD spectra can be simulated by averaging the single conformation spectra using Boltzmann statistics. These single conformation spectra are obtained by Lorentzian broadening (fwhm=10 cm^{-1}) of the calculated discrete line spectra based on dipole and rotational strengths and harmonic vibrational frequencies and are transformed to molar absorptivity units.[49] The conformational populations are calculated on the basis of free energies at room temperature (298.15 K) and can be found in Tables 1 and 2, for the monomer and dimer, respectively. In Figure 5, the calculated single conformation spectra are shown for the C monomer and the CC dimer. It can be seen that there is a significant influence on the IR and VCD spectra due to the dimerization: not only are the dimer intensities systematically higher for both IR and VCD, but also bands of corresponding fundamentals are shifted in frequency.

In Figure 6 the simulated B3LYP/aug-cc-pVTZ monomer (*S*)-**1** and dimer (*SS*)-**1** IR and VCD spectra are compared with experimental IR and half-difference VCD spectra for a 0.42 M solution of (*S*)-(−)-**1** in $CDCl_3$. Both the monomer and dimer spectra have some level of similarity compared to the experiment. By taking both monomer and dimer into account, one can explain the major experimental features.

To interpret the experimental IR and VCD spectra in terms of the DFT results, however, the conformational populations need to be assessed for both monomer and dimer. The theoretical populations based on the free energy differences between monomer and dimer structures are often largely overestimated.[23,50] Nonetheless, information on the fractions of monomer and dimer is embedded in the concentration dependence of the IR band intensities. Using a procedure similar to that described in Chen et al.,[51] it was possible to extract this information by determining the equilibrium constant between monomer and cyclic dimer. The equilibrium for dimerization

$$M + M \rightleftharpoons D$$

is characterized by the dimerization constant $K = [D]/[M]^2$. This constant K can be determined by analyzing the integrated absorbance in function of the analytical concentration of the

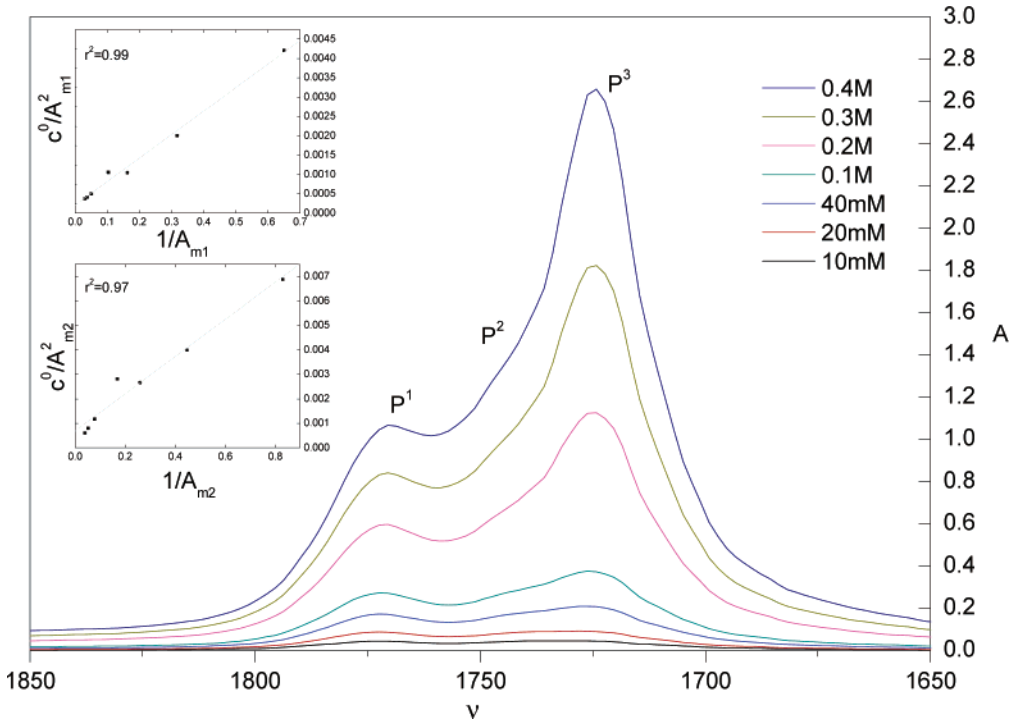

Figure 7. IR spectra of (*R*)-(+)-**1** in $CHCl_3$ for different concentrations varying between 0.4 M and 10 mM. The two subplots represent the linear plot based on eq 2 for band P^1 (top) and band P^2 (bottom). Correlation coefficients are given. Intensities are in absorbance units, frequencies in cm^{-1}.

dissolved species.[51] In this approach, the experimental data are fitted to

$$\frac{c^0}{{A_m}^2} = \frac{1}{\epsilon_m l}\frac{1}{A_m} + \frac{2K}{(\epsilon_m l)^2} \qquad (2)$$

in which c^0/A_m^2 is plotted versus A_m^{-1}. c^0 refers to the analytical concentration of the dissolved species **1**, A_m and ϵ_m are respectively the integrated absorbance and molar absorptivity of a distinct monomer band and l is the path length (0.02 cm).

The model used in this study to approximate the monomer/dimer fractions is based on two individual equilibria between monomer and dimer, that is, an equilibrium between hydrogen bonded monomer (A/B) and the dimer and an equilibrium between the cis configured monomer (C, D, E and F) and dimer.

Several approximations are used: First, the formation of trimers and tetramers and other solute−solute associations are not expected to play a substantial role. Further, possible solvent−solute aggregation is not taken explicitly into account and the concentrations of the $CHCl_3/CDCl_3$ are not exact due to the volatile nature of this solvent. It has also come to our attention that the $CHCl_3$ used in this study contains 0.5 to 1% EtOH for stabilization.[52] The mol fraction EtOH is too low, however, to have any influence on the dimerization equilibrium. Taking into account the aforementioned approximations and limitations of the model, the error on the determined populations is expected to be on the order of 10−15%. However, exact populations are not pursued in this study, but merely tentative values are intended that allow the assessment of experimental IR and VCD in terms of DFT results.

The preferred region to extract population dependent data from the concentration series is the carbonyl stretch region, in which both the monomer and dimer bands are separated and do not coincide with other modes. The OH stretch region is less appropriate as there are many intense solvent bands present and also the CH stretch modes overlap with the dimer OH stretch modes. In Figure 7, the infrared absorbance spectra are given for the concentration series experiment in $CHCl_3$ (same as Figure 4a but in absorbance units). As the solubility of **1** in CS_2 is low, it was difficult to get solutions with accurate concentrations and consequently, the dimerization equilibrium constants for (*R*)-(+)-**1** in CS_2 could not be determined accurately. The integrated intensities for the monomer bands P^1 and P^2 and the dimer band P^3, obtained by Lorentzian fitting, are given in Table 3 for the $CHCl_3$ experiment. If c^0/A_m^2 is plotted versus A_m^{-1} (Figure 7), for the two equilibria defined in our model, the dimerization constants can be determined with eq 2 on the basis of the intercept and the slope of the linear fit. K_1, being the equilibrium constant for the formation of cyclic dimer from monomer A and B, was determined to be 2.7 ($\Delta G_1° = -0.6$ kcal/mol). In the same way, for the equilibrium between the monomers with a cis configured carboxyl (C, D, E and F) and the dimer, K_2 was determined to be 6.9 ($\Delta G_2° = -1.2$ kcal/mol). The predicted free energy difference between conformations A/B and C/D/E/F based on our proposed model is 0.6 kcal/mol. This value agrees reasonably well with the B3LYP/aug-cc-pVTZ free energy difference between conformations B and C, i.e., 0.76 kcal/mol (Table 1).

Defining f_d as the fraction of dimer, f_{m_1} as the fraction of monomer A/B and f_{m_2} as the fraction monomer C/D/E/F, one can write the following expressions for the different fractions within our proposed model

$$f_d + f_{m_1} + f_{m_2} = 1$$

$$(f_{m_1})^2 = f_d \frac{1}{2K_1 c^0}$$

$$(f_{m_2})^2 = f_d \frac{1}{2K_2 c^0} \qquad (3)$$

It is clear that the fractions in eq 3 depend on the analytical

TABLE 3: Integrated Absorbances of CO Stretching Bands from the Monomer, A_{m_1} and A_{m_2}, and Those of Dimer, A_d, for Different Initial Concentrations (c^0 in mol/L) of (*R*)-(+)-1 in $CHCl_3$

c^0	A_{m_1}	A_{m_2}	A_d
0.40	33	26	96
0.30	27	19	69
0.20	20	13	44
0.10	10	6	15
0.04	6	4	9
0.02	3	2	4
0.01	2	1	2

TABLE 4: Experiment Based Populations (B3LYP/aug-cc-pVTZ) for Monomer and Dimer of 1 in $CDCl_3$[a]

	% P		% P		% P		% P
A	23	FC	6	EC	4	ED	3
B	17	D	6	CC	3	FE	2
DC	8	F	6	FD	3	DD	2
C	8	E	6	FF	3	EE	1

[a] $f_{m_1} = 0.40$, $f_{m_2} = 0.25$ and $f_d = 0.35$.

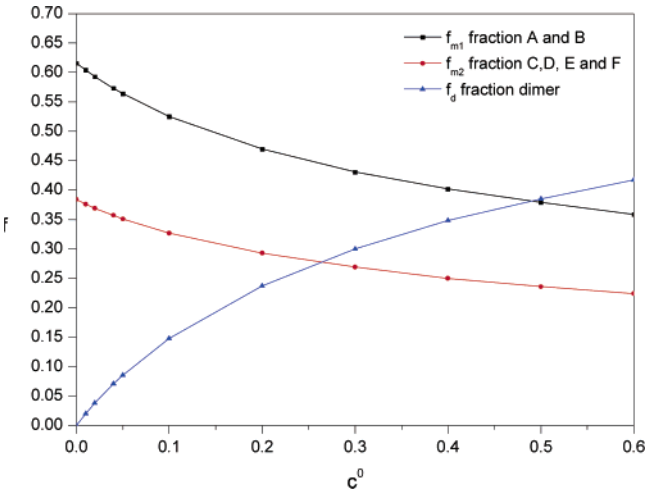

Figure 8. Fractions of monomers A/B (f_{m_1}), C/D/E/F (f_{m_2}) and dimers (f_d) based on experimentally determined values of dimerization equilibrium constants.

concentration for **1**. For a given concentration, the fractions of monomer and dimer can be determined using the obtained equilibrium constants. In Figure 8, the fractions of monomers A/B, C/D/E/F and dimer are given as a function of the analytical concentration c^0. It can be seen that for very small concentrations, only monomer species are present; with the relative concentrations being 62% for A and B and 38% for C, D, E and F. These values compare reasonably well with the B3LYP/aug-cc-pVTZ gas-phase values of 72% and 28% summarized in Table 1.

At a concentration of 0.42 M in $CDCl_3$, which is required to obtain a good VCD S/N ratio, dimer and monomer coexist in solution, from which the fractions present are determined (see Figure 8 and eq 3) to be $f_{m_1} = 0.40$, $f_{m_2} = 0.25$ and $f_d = 0.35$. Based on these values, the populations for the different conformations were determined, taking into account the Boltzmann populations based on the relative free energies of each subgroup of structures, that is, monomer A/B (f_{m_1}), monomer C/D/E/F (f_{m_2}) and dimer (f_d). In Table 4 the experimentally based populations are given for B3LYP/aug-cc-pVTZ data. It has to be mentioned that the experimentally determined equilibrium fractions could be somewhat biased by solvent−solute interaction, which was not taken explicitly into account when modeling the conformations.

The simulated B3LYP/aug-cc-pVTZ and experimental IR and VCD spectra (experimental VCD spectra are half difference spectra) for three different concentrations (0.21, 0.25, and 0.42 M) are shown in Figure 9. The simulated spectra are averaged over all significant dimer and monomer conformations. The populations are calculated by determining the fractions of monomers and dimers for the three different concentrations using eq 3 and taking into account the B3LYP/aug-cc-pVTZ Boltzmann populations. Here, the earlier discussed concentration dependence in the CO stretch region is visible, but a small effect is also seen in the 1300−1400 cm^{-1} area. For the VCD, a more pronounced concentration effect is observed. For higher concentrations, more intense CO stretch dimer bands (fundamental 74 and 73) are observed, but the monomer VCD intensities for fundamentals 29A+B and 27/28 are reduced as are the monomer IR intensities of fundamental 34A+B and 30/29A+B. This obviously indicates that the dimer fraction increases at higher concentrations. The same effects can be observed in the simulated spectra (Figure 9 ii and iv), which indicates that our proposed model works.

In Figure 10 i and iii the experimental IR and half difference VCD spectra for (*S*)-(−)-**1** are given. The infrared region beneath 1000 cm^{-1} has a bad S/N ratio due to the high absorption of $CDCl_3$ in that region. The long-wave cutoff from the optical filter and the CaF_2 windows make that there is no reliable VCD signal observable below 1200 cm^{-1}. Using a different setup with KBr windows and CS_2 as solvent, the spectroscopic window is extended to 800 cm^{-1}. Using CS_2 as solvent, the fractions of monomer appear to be lower than those in $CHCl_3$, but this effect is rather small on the IR and VCD spectrum, as can be seen in Figure S2 in the Supporting Information. Accordingly, the "$CDCl_3$" weighted spectra can be used without any problems for comparison with the experimental CS_2 spectra.

In Figure 10 ii and iv the simulated B3LYP/aug-cc-pVTZ spectra are shown, which are averaged over all the significant (*S*)-**1** monomer and (*SS*)-**1** dimer conformations using the experimental populations given in Table 4 (0.42 M). These simulated spectra can be compared to the experimental (*S*)-(−)-**1** spectra. The B3LYP/aug-cc-pVTZ bands are labeled with their corresponding normal modes. Naturally, monomer and dimer bands overlap, which makes it difficult to assign the bands in much detail. However, where possible, in Figure 10 for monomer and dimer, the bands are assigned to the most contributing conformations (indicated by the conformational label). If the normal modes of different conformations have only a small frequency separation, the conformations are not explicitly mentioned in the labeling. The normal modes of the monomers for the 800−1850 cm^{-1} frequency interval run from 12 to 34, for the dimeric structures from 27 to 73. The monomeric labels are given in black, the dimeric in orange.

In the carbonyl stretching region, a complex pattern can be observed in the IR and in the VCD (Figure 10). The most intense band in the IR can be attributed to the CO asymmetric stretch in the dimer (fundamental 74).

The dimeric CO stretch modes (fundamentals 73 and 74) have lower vibrational frequencies than their monomeric counterpart (fundamental 34). This is due to the hydrogen bonding, which results in a cooperative lengthening of the C═O and OH bonds and a shortening of the C−O bond.[19] Notwithstanding the fact that the calculated frequency splitting between the monomeric and dimeric CO stretch frequencies is somewhat overestimated,

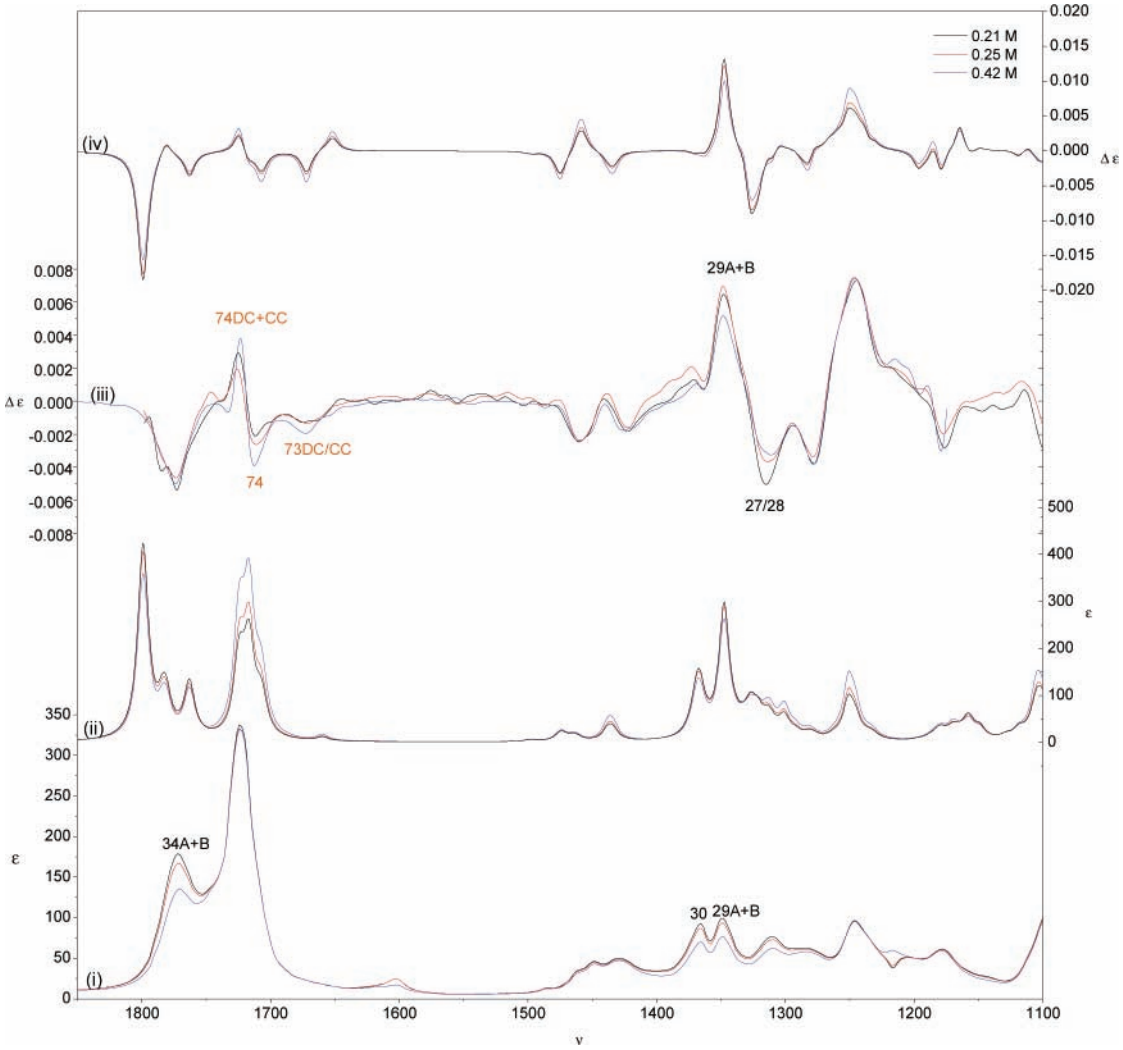

Figure 9. Experimental spectra for (*S*)-(−)-**1** in $CDCl_3$ for three concentrations (0.21, 0.25 and 0.42 M) and B3LYP/aug-cc-pVTZ simulated IR/VCD spectra taking into account monomer and dimer of (*S*)-**1** based on experimental populations for different concentrations (0.21, 0.25 and 0.42 M). Intensities and differential intensities in (differential) molar absorptivity units, frequencies in cm^{-1}.

the IR/VCD for the CO stretching region shows a good agreement with the simulated spectra. Monomeric and dimeric bands can be observed and assigned to calculated bands. Bands 34 from conformations C, D, E and F (34C+D, 34F+E) are unresolved in the IR but can be recognized in the VCD. For the asymmetric CO stretch (mode 73), a negative VCD band is observed, mainly attributable to conformation DC and CC. The other dimer conformations are predicted to have a positive VCD for mode 73, but this cannot be observed in the experimental VCD.

In the spectral region between 1500 and 850 cm^{-1}, a complex spectrum is observed with several unresolved and broad bands. The VCD spectrum in this region has some distinct features, which allows, in combination with the IR spectrum, the assignment of experimental bands. Monomeric fundamentals 29−25 coinciding with dimeric fundamentals 60−56 are not resolved in the IR, which is in agreement with predictions. Some IR bands can be exclusively assigned to dimer structure vibrations, i.e., bands 74, 73, 65, 54DC+CC, 53FC+FD+EC+ED, 46/45, 42/41, 40, and for the VCD, bands 74DC+CC, 74, 74F, 73DC+CC, 73, 65, 54CC+DC, 53FC+FD+EC+ED, 42FF+FD/41, 40, 39. Exclusive monomeric bands in the IR are 34A+B, 34, 30, 19B+F and for the VCD 34A+B, 34C+D, 34 F+E, 27/28, 24, 19A, 19B. The other bands must be assigned to coinciding dimer and monomer fundamentals.

If small differences are neglected, it can be concluded that almost all experimental IR and VCD bands can be assigned with success to the harmonic fundamentals. Some larger bands cannot be observed in the experimental spectra, i.e., VCD band 73 (discussed earlier), VCD band 21A (COH bend), bands 42/41/40 (mainly COH out of plane bend) and VCD band 13/30/29 (CH_2 rocking). As these differences are found for both the 6-31++G** (Supporting Information) and the aug-cc-pVTZ basis set, it is highly unlikely that this is the effect of the use of an incomplete basis set. To investigate the effect of the density functional, six additional functionals (B1LYP, B3P86, B3PW91, B98, MPW1PW91, PBE1PBE) were used to simulate IR and VCD spectra for **1** using the 6-31++G** basis set. These resulting spectra are given in Figures S3 and S4 (Supporting Information). The overall agreement between simulated and experimental spectra is best for the B1LYP and B3LYP functionals. It can also be seen that all the functionals fail to correctly predict the rotational strength of fundamental 73 (selected conformations, see above), fundamental 21 for conformation A, and combined fundamentals 13, 30 and 29. For the B3PW91 and B3P86 functionals, the vibrational frequencies for fundamentals 42, 41 and 40 are shifted somewhat to higher wavenumbers and show a better resemblance with the experimental spectrum for this part of the spectrum compared to the B3LYP functional. However, fundamentals 40, 41 and 42

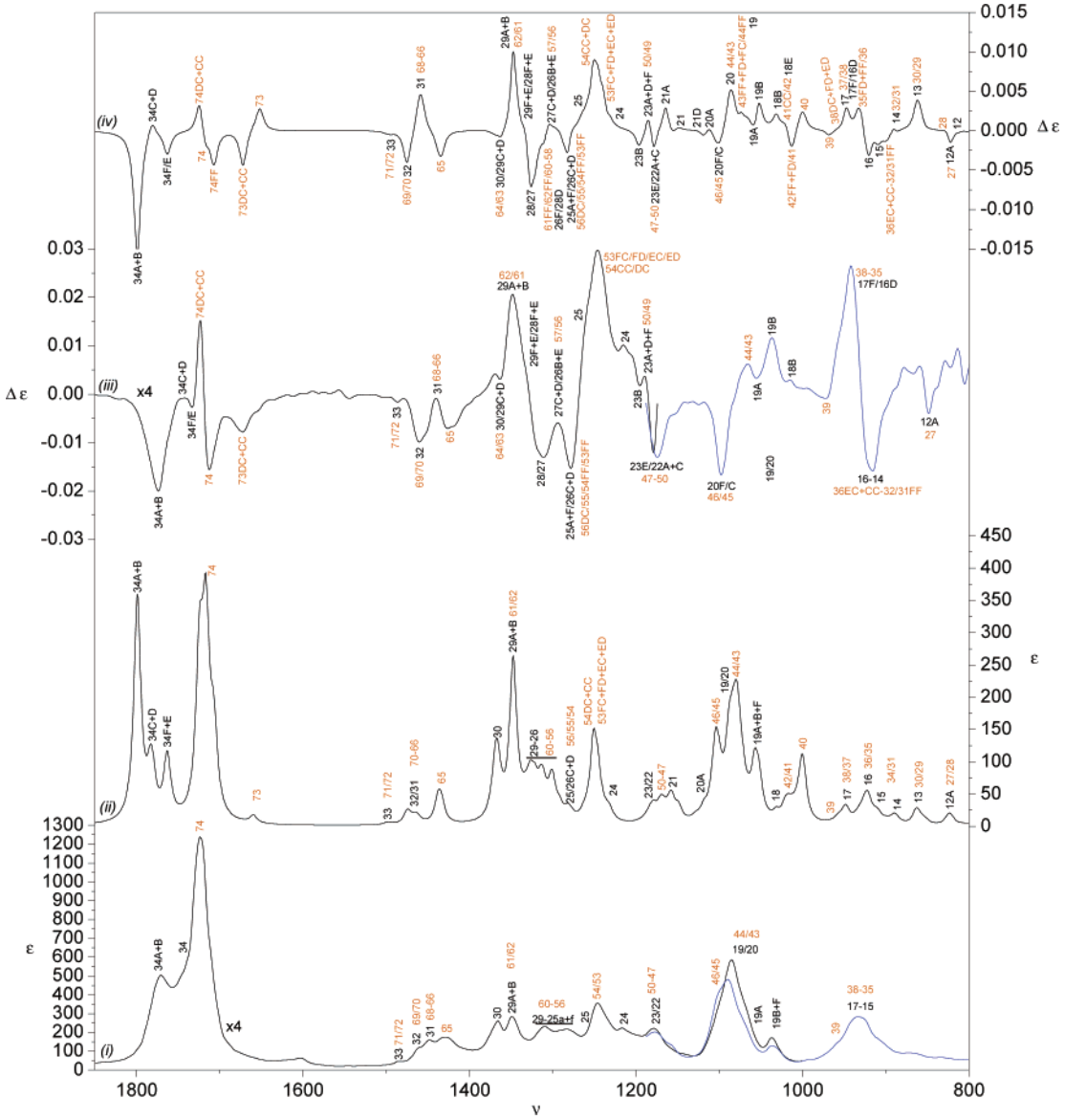

Figure 10. IR (i) and half-difference VCD (iii) spectrum for 0.42M (*S*)-(−)-**1** in $CDCl_3$ (intensities are multiplied with factor 4). For the <1200 cm^{-1} region, the CS_2 spectrum is given (~0.11 M). B3LYP/aug-cc-pVTZ simulated IR (ii) and VCD (iv) spectra taking into account monomer and dimer of (*S*)-**1** based on experimental populations. Intensities (differential) are in molar absorptivity units, frequencies in cm^{-1}.

correspond to COH out of plane bending modes. In a recent study,[54] Antony et al. found that the harmonic COH out-of-plane bending frequency for dimeric benzoic acid is gravely overestimated by ~50 cm^{-1} due to the anharmonic character of this vibrational mode. If this argument is pursued, then it would mean that the predicted frequencies for fundamental 40−42 are overestimated and these would be shifted to lower wavenumbers in the experimental spectra. If these corresponding bands are lowered by 50 cm^{-1}, these would coincide with intense profiles in both IR and VCD bands. This would also explain the relative intensity of the IR band 17−15/38−35.

Taking into account the approximations that are used to determine the monomer and dimer populations to simulate their IR and VCD spectra, it would be of no use to perform a quantitative comparison of simulated and experimental spectra which is sometimes performed,[8,49] for smaller molecules. In this study the situation is even more difficult because not only bands of different conformations, belonging to one species coincide, but also bands from dimer conformations can overlap with bands of the monomer conformations. As a result, no quantitative comparison is performed. However, the assignment of the bands to fundamentals by comparison of the experimental and theoretical spectra was still possible and the resulting agreement in both spectra and trends establishes that for this specific molecule, both monomeric and dimeric species are present and that these can be modeled to simulate spectra.

Conclusions

It this study it is shown that for a carboxylic acid **1** in CS_2 and $CDCl_3$, considerable fractions of monomer exist next to a cyclic dimer, due to the stabilizing effect of an intramolecular hydrogen bonding for two monomer conformations. The equilibrium between the monomer and the cyclic dimer was evaluated using a concentration variation study in $CHCl_3$. The proposed model that describes the equilibrium between intramolecular stabilized monomer and cyclic dimer and non-intramolecular bonded dimer and cyclic dimer predicts monomer equilibrium concentrations that are 60% higher for the stabilized monomer form. The amount of cyclic dimer was found to be dependent on the initial amount of **1** present in $CHCl_3$. Taking into account the equilibrium between monomer and dimer, IR

and VCD spectra were simulated for (*S*)-**1** on the basis of the approximate experimentally determined fractions and B3LYP/aug-cc-pVTZ Boltzmann populations of dimeric and monomeric conformations. Spectra were simulated at the B3LYP/aug-cc-pVTZ level and were compared with experimental spectra for (*S*)-(+)-**1** in $CDCl_3$ and CS_2. A good agreement was obtained, which suggests that the proposed model of dimer/monomer equilibrium is valid within the scope of our article.

Acknowledgment. The Fund for Scientific Research-Flanders (FWO-Vlaanderen) is thanked for financial support for the spectroscopic equipment and the computational facilities used in this study. Financial support allowing the purchase of the computer cluster CalcUA was obtained through the "Impulsfinanciering" provided by the Flemish Government.

Supporting Information Available: B3LYP/6-31++G** and cc-pVTZ conformational description for monomer of **1** and 6-31++G** description for dimer of **1**. Monomer and dimer aug-cc-pVTZ normal modes. The CO and OH stretching region for solutions of (*R*)-(+)-**1** in CS_2. $CDCl_3$ and CS_2 simulated and experimental spectra. Simulated IR/VCD DFT/6-31++G** spectra for different functionals. This material is available free of charge via the Internet at http://pubs.acs.org.

References and Notes

(1) Fujima, Y.; Hirayama, Y.; Ikunaka, M.; Nishimoto, Y. *Tetrahedron-Asymm.* **2003**, *14* (10), 1385−1391.

(2) Ishigura, M.; Nishihara, T.; Tanaka, R. *Yakugaku Zasshi* **2001**, *121* (12), 915−927.

(3) Hoffman-Roberts, H. L.; Babcock, E. C.; Mitropoulos, I. F. *Expert Opin. Invest. Drugs* **2005**, *14* (8), 973−995.

(4) Ayers, P. W.; Yang, W. Density-functional theory. In *Computational medicinal chemistry for drugs discovery*; Bultinck, P., De Winter, H., Langenaeker, W., Tollenaere, J. P., Eds.; Marcel Dekker: New York, 2004; pp 89−118.

(5) Cheeseman, J. R.; Frisch, M. J.; Devlin, F. J.; Stephens, P. J. *Chem. Phys. Lett.* **1996**, *252* (3−4), 211−220.

(6) Devlin, F. J.; Stephens, P. J.; Cheeseman, J. R.; Frisch, M. J. *J. Phys. Chem. A* **1997**, *101* (51), 9912−9924.

(7) Stephens, P. J.; Ashvar, C. S.; Devlin, F. J.; Cheeseman, J. R.; Frisch, M. J. *Mol. Phys.* **1996**, *89* (2), 579−594.

(8) Aamouche, A.; Devlin, F. J.; Stephens, P. J. *J. Am. Chem. Soc.* **2000**, *122* (10), 2346−2354.

(9) Devlin, F. J.; Stephens, P. J.; Scafato, P.; Superchi, S.; Rosini, C. *Tetrahedron-Asymm.* **2001**, *12* (11), 1551−1558.

(10) Dyatkin, A. B.; Freedman, T. B.; Cao, X. L.; Dukor, R. K.; Maryanoff, B. E.; Maryanoff, C. A.; Matthews, J. M.; Shah, R. D.; Nafie, L. A. *Chirality* **2002**, *14* (2−3), 215−219.

(11) Kuppens, T.; Langenaeker, W.; Tollenaere, J. P.; Bultinck, P. *J. Phys. Chem. A* **2003**, *107* (4), 542−553.

(12) Kuppens, T.; Vandyck, K.; Van der Eycken, J.; Herrebout, W.; van der Veken, B. J.; Bultinck, P. *J. Org. Chem.* **2005**, *70* (23), 9103−9114.

(13) Wang, F.; Polavarapu, P. L. *J. Phys. Chem. A* **2000**, *104* (9), 1822−1826.

(14) Stephens, P. J. Vibrational circular dichroism spectroscopy: A new tool for the stereochemical characterization of chiral molecules. In *Computational medicinal chemistry for drugs discovery*; Bultinck, P., De Winter, H., Langenaeker, W., Tollenaere, J. P., Eds.; Marcel Dekker: New York, 2004; pp 699−725.

(15) Nafie, L. A. *Appl. Spectrosc.* **2000**, *54* (11), 1634−1645.

(16) Kuppens, T.; Bultinck, P.; Langenaeker, W. *Drug Discovery Today: Technol.* **2004**, *1* (3), 269−275.

(17) Kollman, P. A.; Allen, L. C. *Chem. Rev.* **1972**, *72* (3), 283−303.

(18) Patai, S. *The Chemistry of acid derivatives*; Wiley: New York, 1992.

(19) Wolfs, I.; Desseyn, H. O. *J. Mol. Struct. (THEOCHEM)* **1996**, *360*, 81−97.

(20) Lewell, X. Q.; Hillier, I. H.; Field, M. J.; Morris, J. J.; Taylor, P. J. *J. Chem. Soc., Faraday Trans. Ii* **1988**, *84*, 893−898.

(21) Devlin, F. J.; Stephens, P. J. *J. Am. Chem. Soc.* **1999**, *121* (32), 7413−7414.

(22) Wang, F.; Polavarapu, P. L.; Lebon, F.; Longhi, G.; Abbate, S.; Catellani, M. *J. Phys. Chem. A* **2002**, *106* (51), 12365−12369.

(23) Cappelli, C.; Corni, S.; Mennucci, B.; Cammi, R.; Tomasi, J. *J. Phys. Chem. A* **2002**, *106* (51), 12331−12339.

(24) Wang, F.; Polavarapu, P. L. *J. Phys. Chem. A* **2000**, *104* (46), 10683−10687.

(25) He, J. T.; Polavarapu, P. L. *J. Chem. Theory Comput.* **2005**, *1* (3), 506−514.

(26) Urbanova, M.; Setnicka, V.; Devlin, F. J.; Stephens, P. J. *J. Am. Chem. Soc.* **2005**, *127* (18), 6700−6711.

(27) Cervinka, O.; Bajanzulyn, O.; Fabryova, A.; Sackus, A. *Collect. Czech. Chem. Commun.* **1986**, *51* (2), 404−407.

(28) Urbanova, M.; Setnicka, V.; Volka, K. *Chirality* **2000**, *12* (4), 199−203.

(29) Spectrogon AB, Taeby, Sweden; www.spectrogon.com.

(30) Aamouche, A.; Devlin, F. J.; Stephens, P. J.; Drabowicz, J.; Bujnicki, B.; Mikolajczyk, M. *Chem.—Eur. J.* **2000**, *6* (24), 4479−4486.

(31) Frisch, M. J.; Trucks, G. W.; Schlegel, H. B.; Scuseria, G. E.; Robb, M. A.; Cheeseman, J. R.; Montgomery, J. A., Jr.; Vreven, T.; Kudin, K. N.; Burant, J. C.; Millam, J. M.; Iyengar, S. S.; Tomasi, J.; Barone, V.; Mennucci, B.; Cossi, M.; Scalmani, G.; Rega, N.; Petersson, G. A.; Nakatsuji, H.; Hada, M.; Ehara, M.; Toyota, K.; Fukuda, R.; Hasegawa, J.; Ishida, M.; Nakajima, T.; Honda, Y.; Kitao, O.; Nakai, H.; Klene, M.; Li, X.; Knox, J. E.; Hratchian, H. P.; Cross, J. B.; Bakken, V.; Adamo, C.; Jaramillo, J.; Gomperts, R.; Stratmann, R. E.; Yazyev, O.; Austin, A. J.; Cammi, R.; Pomelli, C.; Ochterski, J. W.; Ayala, P. Y.; Morokuma, K.; Voth, G. A.; Salvador, P.; Dannenberg, J. J.; Zakrzewski, V. G.; Dapprich, S.; Daniels, A. D.; Strain, M. C.; Farkas, O.; Malick, D. K.; Rabuck, A. D.; Raghavachari, K.; Foresman, J. B.; Ortiz, J. V.; Cui, Q.; Baboul, A. G.; Clifford, S.; Cioslowski, J.; Stefanov, B. B.; Liu, G.; Liashenko, A.; Piskorz, P.; Komaromi, I.; Martin, R. L.; Fox, D. J.; Keith, T.; Al-Laham, M. A.; Peng, C. Y.; Nanayakkara, A.; Challacombe, M.; Gill, P. M. W.; Johnson, B.; Chen, W.; Wong, M. W.; Gonzalez, C.; Pople, J. A. *Gaussian03*, revision B.05; Gaussian, Inc.: Wallingford, CT, 2004.

(32) Becke, A. D. *J. Chem. Phys.* **1993**, *98* (7), 5648−5652.

(33) Lee, C. T.; Yang, W. T.; Parr, R. G. *Phys. Rev. B—Condens. Matter* **1988**, *37* (2), 785−789.

(34) Stephens, P. J.; Devlin, F. J.; Chabalowski, C. F.; Frisch, M. J. *J. Phys. Chem.* **1994**, *98* (45), 11623−11627.

(35) Sander, W.; Gantenberg, M. *Spectrochim. Acta A* **2005**, *62* (4−5), 902−909.

(36) Sadlej, J.; Dobrowolski, J. C.; Rode, J. E.; Jamroz, M. H. *Phys. Chem. Chem. Phys.* **2006**, *8* (1), 101−113.

(37) Frisch, A. E.; Frisch, M. J.; Trucks, G. *Gaussian 03 User's Reference*, 5th ed.; Gaussian, Inc.: Pittsburgh, 2003.

(38) Ditchfield, R. *Mol. Phys.* **1974**, *27* (4), 789−807.

(39) Stephens, P. J. *J. Phys. Chem.* **1987**, *91* (7), 1712−1715.

(40) McQuarrie, D. A. *Statistical Thermodynamics*; Harper and Row: New York, 1973.

(41) Hehre, W. J.; Radom, L.; Schleyer, P. R.; Pople, J. A. *Ab initio molecular orbital theory*; Wiley: New York, 1986.

(42) Allinger, N. L.; Yuh, Y. H.; Lii, J. H. *J. Am. Chem. Soc.* **1989**, *111* (23), 8551−8566.

(43) Allinger, N. L.; Chen, K. S.; Lii, J. H. *J. Comput. Chem.* **1996**, *17* (5−6), 642−668.

(44) Halgren, T. A. *J. Comput. Chem.* **1996**, *17* (5−6), 490−519.

(45) Cremer, D.; Pople, J. A. *J. Am. Chem. Soc.* **1975**, *97* (6), 1354−1358.

(46) Wu, A.; Cremer, D. *J. Phys. Chem. A* **2003**, *107* (11), 1797−1810.

(47) Fernandez, L. E.; Marigliano, A. C. G.; Varetti, E. L. *Vibr Spectrosc.* **2005**, *37* (2), 179−187.

(48) Eliason, T. L.; Havey, D. K.; Vaida, V. *Chem. Phys. Lett.* **2005**, *402* (1−3), 239−244.

(49) Kuppens, T.; Herrebout, W.; van der Veken, B. J.; Corens, D.; De Groot, A.; Doyon, A.; Van Lommen, G.; Bultinck, P. *Chirality* **2006**, *18*(8), 609−620.

(50) Yu, Y. B.; Privalov, P. L.; Hodges, R. S. *Biophys. J.* **2001**, *81* (3), 1632−1642.

(51) Chen, J. S.; Wu, C. C.; Kao, D. Y. *Spectrochim. Acta A* **2004**, *60* (10), 2287−2293.

(52) Zhao et al.[53] describe that the polypeptide gramicidin undergoes dimerization in solution. Gramicidin is reported to have a different VCD in $CDCl_3$ compared to $CHCl_3$ solutions (which contains 1% EtOH) in the amide I region. Their IR signatures are the same in this region.

(53) Zhao, C. X.; Polavarapu, P. L. *Biospectroscopy* **1999**, *5*, 276−283.

(54) Antony, J.; von Helden, G.; Meijer, G.; Schmidt, B. *J. Chem. Phys.* **2005**, *123* (1).